TRANSIENT THERMAL ANALYSIS OF AN INDUCTION ELECTRIC MOTOR

Cassiano Antunes Cezário
WEG Industries – Motors (Jaraguá do Sul, Santa Catarina – Brazil) / Federal University of Santa Catarina - UFSC
cassiano@weg.com.br

Marcelo Verardi
WEG Industries – Motors (Jaraguá do Sul, Santa Catarina – Brazil) / Federal University of Santa Catarina - UFSC
marcelov@weg.com.br

Samuel Santos Borges
WEG Industries – Motors (Jaraguá do Sul, Santa Catarina – Brazil)
samuelb@weg.com.br

Jonny Carlos da Silva
Federal University of Santa Catarina - UFSC (Florianópolis, Santa Catarina – Brazil)
jonny@emc.ufsc.br

Amir Antônio Martins Oliveira
Federal University of Santa Catarina - UFSC (Florianópolis, Santa Catarina – Brazil)
amirol@emc.ufsc.br

Abstract. *This paper presents a thermal circuit model to simulate the behavior of an electric motor during the transient duty leading to steady-state operation under rated load. The proposed model allows the calculation of the temperature distribution in the radial direction of the electric motor, from the shaft inside to the motor frame surface. Several heat sources inside the motoras well as the heat conduction and the thermal contact resistances have been considered. The surface convection heat transfer inside the motor and at its external surfaces is modeled by using heat transfer coefficients. In the longitudinal direction, only the convection resistances inside the motor were considered. Due to its flexibility and ease of implementation, the software* AMESim® *was used as the platform for modeling and simulation. The experiments has been carried out with a 37 kW WEG motor, and the simulated results reproduced the experimental behavior properly. The simulation points out the importance for a correct modeling of internal heat generation and contact resistances in order to predict the transient behavior.*

Keywords*: heat transfer, electric motor, thermal circuit simulation, AMESim*â.

1. Introduction

The prediction of the temperature distribution inside an operating electric motor is one of the most important issues during its design. This prediction allows the engineer to evaluate if the machine will reach the thermal class for which it is being designed, establishing the bearing lubrication intervals as well as checking if the supplied air flow of the cooling system is sufficient for ensuring normal motor operation at rated conditions.

Several works have been done for the electric motor modeling. Most of these works are based on thermal circuit modeling (Saari, 1998; Bousbaine, 1999; Staton et al., 2001; El-Refaie et al., 2002). These works allow to predict the overall motor temperature variation and distribution, can be used for determining the effects of different designs, duties and cooling mechanisms of the motor temperature during its operation. Detailed analysis of fluid flow and heat transfer with finite volumes and finite elements are also available (Staton et al., 2001; El-Refaie et al., 2002). Some works also couple the temperature field determination with the electric and magnetic fields inside electric motors (Chauveau et al., 2002).

This paper presents a thermal circuit model of an electric motor aiming to simulate its thermal behavior during the transient duty towards steady-state operation at rated load. The model is applied to a specific induction electric motor and the predictions are compared to measurements. The purpose of the model is to become an integral part of the motor design process aiming to optimize components and manufacturing processes.

2. Description of the Analysed Motor

The electric motor to be modeled is an ABNT 200L (ABNT NBR-5432), IV poles, 37 kW, 60 Hz, B3 mount (ABNT CB-20) motor manufactured by WEG Industries – Motors, Jaraguá do Sul, SC, Brazil. Figure 1 shows a detailed view of the main components of the modeled electric motor. The modeling is focused on the frame, the stator

and the rotor. This motor type has copper windings in the stator and both stator and rotor are made of steel plate laminations referred hereinafter as iron.

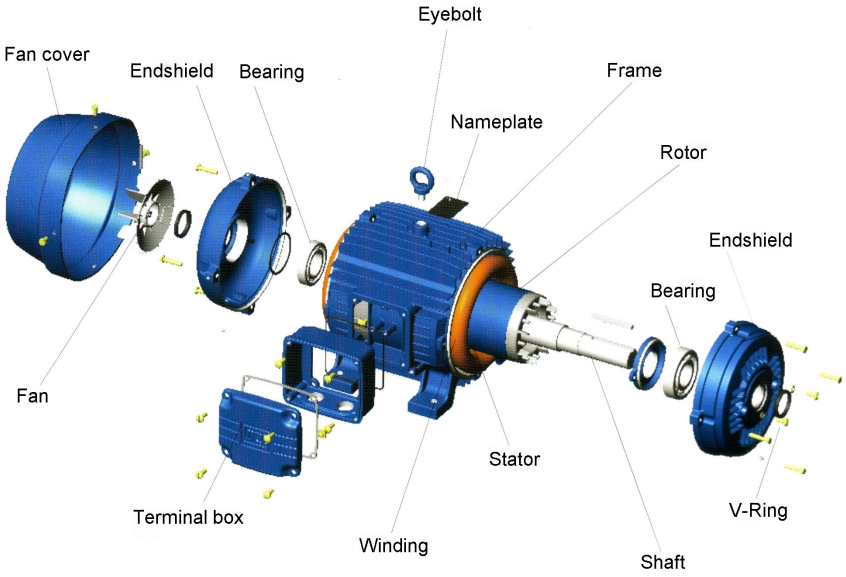

Figure 1. View of the components that form the electric motor under analysis.

3. Mechanisms of Heat Generation inside an Induction Electric Motor

The main mechanisms of heat generation in induction electric motors are generally divided in four groups, related mainly to the places where they occur. These are Joule losses, iron losses, stray load losses and mechanical losses. Each one of these kinds of energy conversion from electric to thermal energy is detailed below.

3.1 Joule Losses

This mechanism corresponds to the conversion of electric energy into thermal energy in electrical conducting media. This type of losses is directly related to the electric resistance of the conductor and changes proportionally to the square of the current, i.e., $Pj = R*I^2$. Energy conversion by Joule effect in squirrel cage induction electric motors occurs in the stator (copper windings) and in the squirrel cage (aluminum bars).

3.2 Iron Losses

These losses are due to the conversion of electric energy into thermal energy in the iron. They are divided in hysteresis and Foucault (eddy currents) losses. The eddy-current losses are Joule losses that occur in the iron due to the flow of an induced electric current. The hysteresis losses are due to the energy expended to align the iron magnetic poles to the applied magnetic field and their order of magnitude corresponds to the area of the hysteresis loop in the electrical induction (***B***) versus magnetic field (***H***) plot (Figure 2).

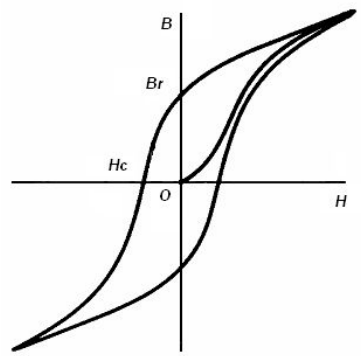

Figure 2. Plot of the electric induction (***B***) versus magnetic field (***H***) for the iron.

3.3 Stray load losses

The stray load losses are minor losses in the electric motor operation and their quantification is very difficult. They include the losses due to the skin effect, high frequency, among others, that are unknown or not easily quantified.

3.4 Mechanical losses

These losses comprise the conversion of the mechanical energy into thermal energy due to mechanical friction and viscous losses. Here are included mainly the losses in the rolling bearings (balls/rings interface) and the cooling fan losses. The cooling fan losses are due to the mechanical energy required for blowing air over the motor surface, including the conversion of air kinetic energy, flow work and viscous dissipation.

3.5 Contribution of Each Group

For the correct modeling, it is important to quantify the suitable value and location of the heat generation. In general, the quantification of the losses is directly related to the location where these losses occur in the electric motor, excepting the stray losses. Figure 3 shows the distribution of these losses and the respective locations where they occur. The values are shown in a relative scale.

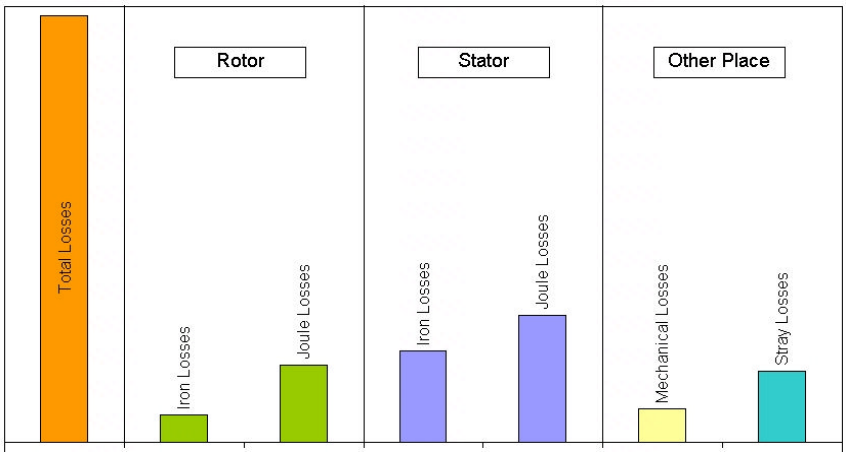

Figure 3. Contribution of each group to the total losses and the respective locations where they occur (relative scale).

This information is used as an input in the model. No effort is required to calculate these losses directly from the calculation of the electric and magnetic fields distribution within the electric motor.

4. Description of the Thermal Circuit Model

The model developed allows the calculation of the radial distribution of temperatures, from the shaft to the frame. In the longitudinal direction only the surface convection resistances in the interior of the electric motor have been considered, i.e., the forced convection resistances due to the rotor rotation and the convection around the motor end-windings, admitted as natural convection.

Based on WEG experience, it is known that the proper evaluation of the thermal contact resistances between the shaft and the rotor steel lamination stack and the evaluation of the surface convection coefficients are critical. In this model, the surface convection coefficients have been obtained from empirical correlations available in the literature (Kaviany, 2001; Incropera and DeWitt, 1998) and the contact resistances are calculated from empirical correlations developed at WEG, for this class of electric motors.

Figure 4 shows the motor thermal model sketch as built with AMESim® libraries. This is a software available from Imagine, France. Basically the model is formed by eight thermal capacitances, which represent the shaft, the rotor steel lamination stack, the aluminum of the rotor squirrel cage, the copper of the windings, the stator steel lamination stack and the frame of the electric induction motor. The rotor steel lamination stack and the stator steel lamination stack are represented by two thermal capacitances. This is used due to the construction of the electric motor and due to the assumption that the heat flow in the rotor steel lamination does not cross only through the aluminum of the squirrel cage, but rather there is an additional parallel path through the neighbouring rotor steel lamination. The same consideration is made for the stator steel lamination and the copper winding.

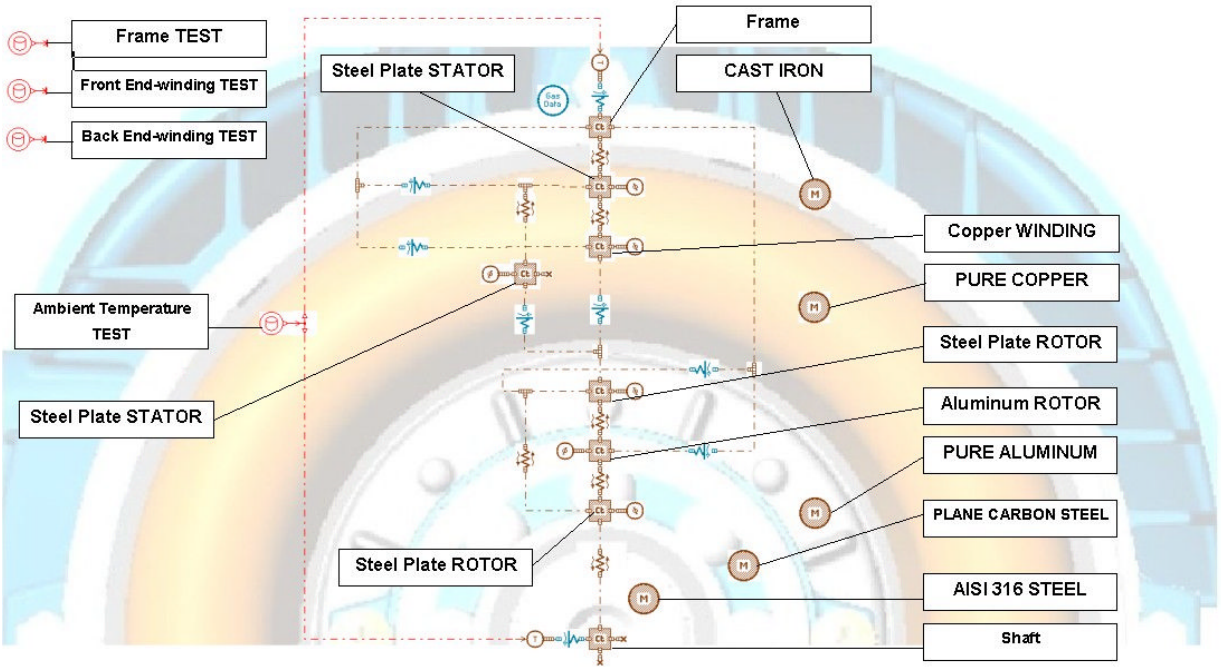

Figure 4. Model sketch built in AMESim® showing the components (listed in section 6.1) of the thermal circuit.

The model considers that the ambient temperature during a typical test may vary, and it is used as input. The thermophysical properties of the air and metal components evaluated at ambient temperatures are already implemented in the software.

5. Correlations for Surface Convection Heat Transfer

A forced convection heat transfer is assumed for the side rotor and ring surfaces of the squirrel cage. Kaviany (2001) presents a correlation for the Nusselt number of a rotating disc in an initially quiescent medium based on the disc radius given by

$$Nu_r = \frac{0.585 * Re_r^{1/2}}{\frac{0.6}{Pr} + \frac{0.95}{Pr^{1/3}}} \quad \text{Valid for } Re < 2.4 \times 10^5 \tag{1}$$

Where:
Nu_r = the Nusselt number;
Re_r = the Reynolds number;
Pr = the Prandtl number.

The Nusselt number for the surface convection heat transfer in the fluid filling the space between the rotor and the stator is obtained from (Kaviany, 2001)

$$Nu_r = 0.027 * Re_r^{0.805} * Pr^{1/3} \quad \text{Valid for } 4 \times 10^4 < Re < 4 \times 10^5 \tag{2}$$

Since the shaft rotates, the Nusselt number for the surface convection at the shaft surface is obtained from (Kaviany, 2001)

$$Nu_r = 0.193 * Re_r^{0.618} * Pr^{1/3} \quad \text{Valid for } 4 \times 10^3 < Re < 4 \times 10^4 \tag{3}$$

For the frame, the fan generates a forced turbulent flow in axial direction. The Nusselt number is obtained by (Incropera and DeWitt, 2003) assuming a turbulent flow over a flat plate

$$Nu_r = 0.0296 * Re_r^{0.8} * Pr^{1/3} \text{ Valid for } Re < 10^8 \quad (4)$$

For the correlation for the natural convection that occurs on the surface of the end-windings and on the inner stator surface of the electric motor, the default value of the software was used.

6. Implementation in AMESimâ

6.1 Libraries

The AMESim® 4.3.1 software is an environment for modeling of multi-domain systems, i.e. thermal, hydraulic, pneumatic, mechanical and electrical systems. It uses a multiport approach to transfer information from one component to another arranged in a network. It has different suitable libraries of components for specific applications. Each component is characterized by input and output variables (information), a set of internal functions that describe the treatment of these variables and the internal parameters that describe properties. In the thermal model, the inputs and outputs are temperatures and heat transfer rates. The internal functions are the energy equation and equations for thermal resistances and heat transfer rates and the internal parameters are the thermophysical properties. The way the components connect to each other is like a standard thermal circuit model (Kaviany, 2001). The components used to perform this implementation are shown below (Imagine, 2000).

6.1.1 Thermal library

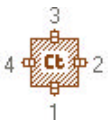

THC00 - Thermal capacitance: The submodel used has 4 thermal ports, where the inputs are heat flow values [W]. It uses the values of temperature [°C] as state variables. Eight submodels of this type were used to represent different components of the electric motor.

THCD4 - Contact conductive exchange: This submodel has 2 thermal ports, where the heat flow [W] is the output value and the inputs are the two end temperatures. These resistances are used to represent the heat transfer between two materials in mechanical contact.

THHS0 - Constant heat flow: This submodel is used to set the heat generation in the thermal capacitances due to conversion from other energy forms to thermal energy. This submodel allows only the value specification of the heat transfer rate to the thermal capacitance [W].

THTC0 - Conversion of signal to temperature: Another submodel converts a signal into temperature. Here, the variations of the ambient temperature recorded during the experiments are converted to temperature input for the model.

TH_XX - Thermal solid properties: The submodel, containing the thermophysical properties of the solid materials, is linked to the corresponding thermal capacitances through one internal index. Thus, different materials can be integrated in a same model, as for our analyzed motor.

6.1.2 Thermal pneumatic library

TPGD3 - Perfect gas characteristics: The submodel has the thermophysical properties of the gas (air) and is linked to the corresponding thermal components through one internal index.

TPCV05 - External flow forced convective exchange: This submodel describes the forced convection heat transfer resistance. It has the two temperatures [°C] as input and the heat transfer rate [W] as output.

6.1.3 Library of signals

UDA1 - Signal form ASCII file data: This submodel allows to read data from a file with the "txt" extension. This signal is used to read the values of the ambient temperature.

6.2 Simulation Parameters for AMESim[â]

The total simulation time was 12690 seconds, which corresponds to the time required for the motor to reach the steady-state temperature at full load. The calculated temperatures are stored every 10 seconds. AMESim® uses a modified version of the LSODA algorithm. Internally, the program chooses an ADAMS algorithm when the ordinary differential equations are non-stiff and a GEAR algorithm when they are stiff. The adopted error tolerance in the numerical simulation was 10^{-8}, since tests with smaller tolerances provided no significant improvement in the test results.

7. Validation

For the model validation, an experimental test was performed with the same electric motor that has been used for the model development. The electric motor has been tested under rated load conditions at 380 V. A Yokogawa graphic multichannel recorder model LR8100E with 8 channels was used to record the temperatures from 5 different types of thermocouples. Figure 5 shows the arrangement of the experimental setup at WEG laboratory, indicating the data recorder (1) and the motor (2).

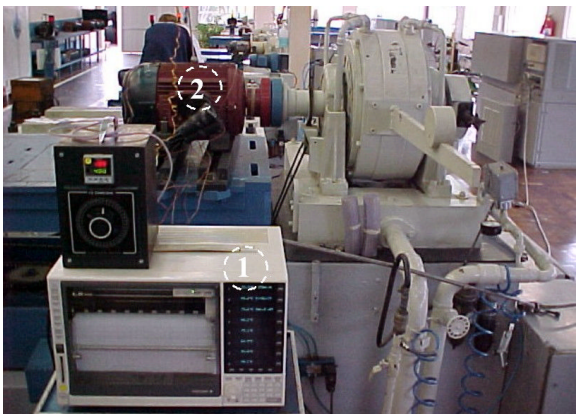

Figure 5. Experimental setup showing the data recorder (1) and the electric motor (2) coupled to a dynamometer.

Table 1 lists the locations of the thermocouples. All are mounted in stationary components. A total measurement error (thermocouple wire and bead, data acquisition and compensation, installation effects) of ± 1°C is estimated.

Table 1. Description of the location of the thermocouples.

Thermocouple number	Location
01	DE end-winding
02	NDE end-winding
03	Eyebolt fixing hole
04	DE Inner bearing cap
05	NDE Inner bearing cap

8. Results

Table 2 shows a summary of the steady-state results recorded during the experiment and calculated from the model. The difference between the measurements and the analysis is below 5% and within the estimated measurement error.

Table 2. Comparison between measured and calculated temperatures.

Thermocouple location	Calculated (°C)	Measured (°C)	Difference (%)
DE end-winding	102.6	106.0	+ 3.2
NDE end-winding.	102.6	98.0	- 4.7
Eyebolt fixing hole	69.8	68.0	- 2.6
DE Inner bearing cap	69.1	73.0	+ 5.3
NDE Inner bearing cap	69.1	67.0	- 3.1

Averaging the temperatures measured at the DE and NDE end-windings and comparing this average to the calculated temperature, the difference reduces to 0.5%. In a similar way, averaging the measured temperatures on the DE inner bearing cap and the NDE bearing cap and comparing them to the calculated temperature, the difference reduces to 1.2%. This comparison provides very accurate results, when we consider that the model does not deal with the longitudinal direction in detail.

Figure 6 shows the calculated and the measured values considering the time variation of the winding temperature. The continuous line indicates the calculated temperature and the dashed lines indicate measured temperatures of the DE and NDE end-windings. The model enables us to predict in a suitable manner the time evolution of the winding temperatures. We can also note that the winding temperature is not very much affected by the surface convection heat transfer and that this winding temperature depends mainly on the values of heat generation and thermal contact resistance used in the model. The results show that the used values are suitable for this motor.

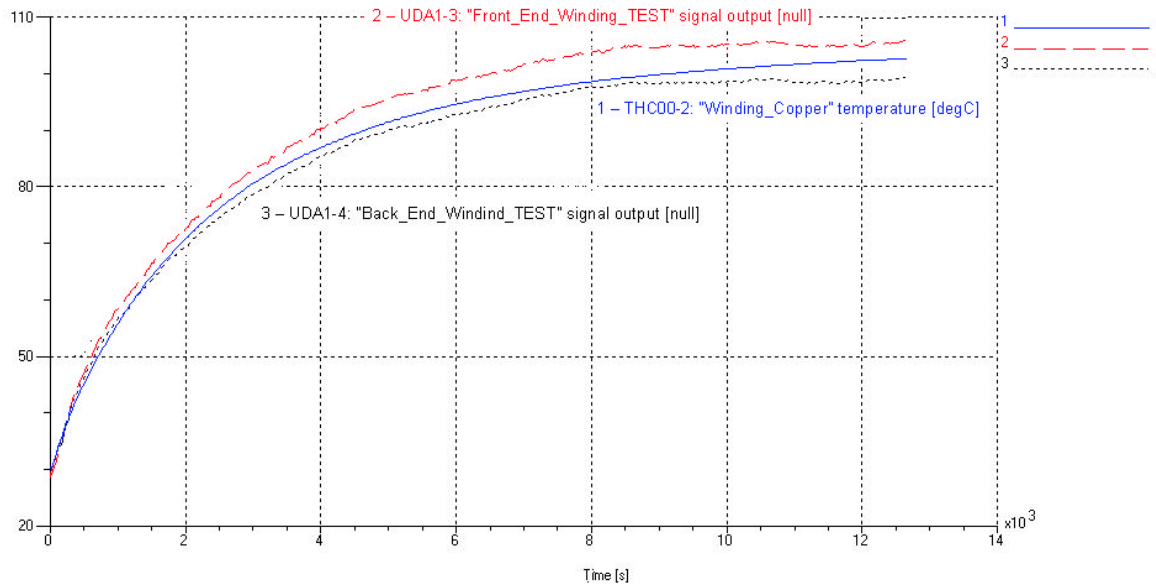

Figure 6. Time variation of the calculated and measured temperatures for the DE and NDE end-windings.

Figure 7 shows the time variation of the calculated and measured frame temperatures. Although the measured temperature shows a short delay as a result of a slight advance in the start of the data recording, in general there is a good agreement between the calculated and measured values. However, the above model predicts an initial temperature rise. This may be due to the fact that the surface convection coefficients are not totally suitable for the initial temperature rise or are caused by and insignificant delay in the heat generation while the motor is speeding up. As soon as the temperature converges to a steady-state condition, we note that the derivatives of the measured and calculated temperatures match very well.

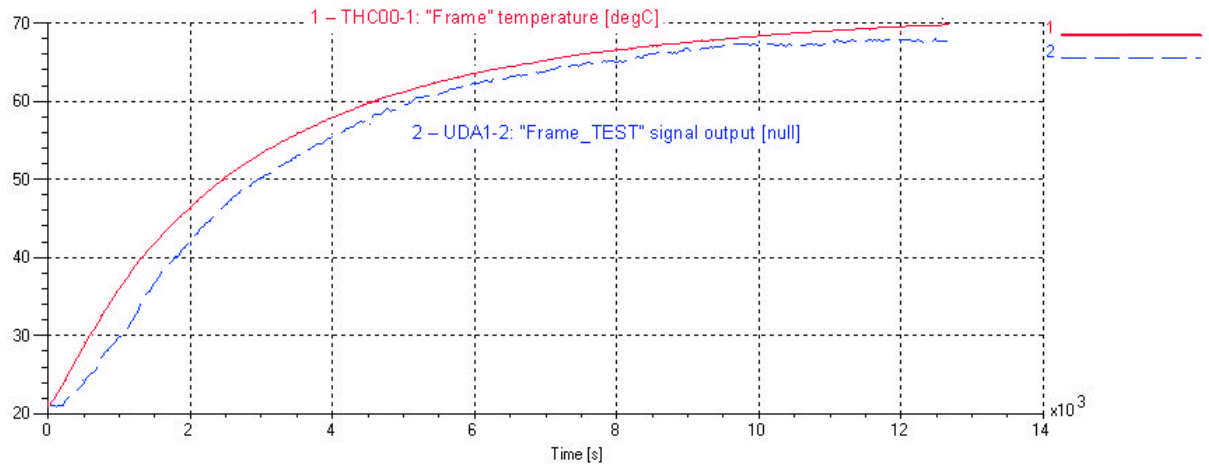

Figure 7. Time variation of the calculated and measured frame temperatures.

9. Conclusion

The developed model predicts in a suitable manner the overall behavior of the motor temperatures during the transient and steady-state operation. The model shows that for a global prediction of temperatures in an induction electric motor (averaged surface and volumetric temperatures), it is more important to account properly for the radial heat transfer, heat generation distribution, contact conductance and surface convection modeling than to account for a detailed longitudinal heat transfer modeling. From these models, the heat transfer and surface convection can rely on available models in the literature. The heat generation and contact resistance, however, must rely on specific models specially developed for the motor under analysis. The contact resistance, in particular, depends strongly on the manufacturing techniques, which are specific for each motor design. Also, local surface and volumetric temperatures require more complete modeling of the heat transfer in the solid and fluid. The conductance across the contact between the motor components and the surface convection heat transfer at rotating and ventilated parts are current research topics.

However, the universe of types and designs of electric motors is large and all studies depend strongly on the geometrical, manufacturing and thermophysical characteristics of the specific electric motor under study, and therefore very few general conclusions can be extracted aiming to improve other motor designs.

The AMESim® software proved to be a useful tool for thermal circuit modeling, especially for electric induction motors. Its user-friendly graphic interface allows easy set up and solution of the model. Then the designer can focus on the physical aspects of the design, leaving the programming and mathematical aspects to AMESim®.

10. Acknowledgements

The authors gratefully acknowledge WEG Industries – Motors for allowing the development of this work and the Graduate Program in Design of Electrical Machines developed as partnership among the Mechanical Engineering Department at UFSC, Florianópolis, SC, UNERJ, Jaraguá do Sul, SC, and WEG Industries – Motors, Jaraguá do Sul, SC.

11. References

Bousbaine, A., 1999, “Thermal Modelling of Induction Motors Based on Accurate Loss Density Distribution”, Electric Machines and Power Systems, 14 p.

Chauveau, E., Zaïm, M. E., Saïdi, T., Trichet, D. and Fouladgar, J., 2002, “Magneto-Thermal Modeling of Induction Machines Using Inverse Problem Methodology”, J. Phys. III, pp.1849-1859.

Imagine, 2000, “AMESim® - A Brief Technical Overview”, Technical Bulletin no. 100, IMAGINE S.A., Roanne, France, available at: www.amesim.com

Incropera, F.P. and De Witt, D.P., 2003, “Fundamentos de Transferência de Calor e Massa”, LTC - Livros Técnicos e Científicos S.A., Rio de Janeiro, Brasil, 698 p.

Kaviany, M., 2001, “Principles of Heat Transfer”, John Wiley & Sons Inc., New York, United States of America, 973 p.

Martin, J.C.,1982, “Cálculo Industrial de Máquinas Eléctricas”, Marcombo S.A., Barcelona, España, 590 p.

Saari, J., 1998, “Thermal Analysis of High-Speed Induction Machines”, Acta Polytechnica Scandinavica, Electrical Engineering Series No. 90, Published by the Finnish Academy of Technology, Helsinki, 73 p.

Staton, D., Pickering, S. and Lampard, D., 2001, “Recent Advancement in the Thermal Design of Electric Motors”, Proceedings of the SMMA 2001 Fall Technical Conference “Emerging Technologies for Electric Motion Industry”, Durham, North Carolina, USA, 3-5 Oct., 11 p.

Xypteras, J. Maras, K., Spyrelis, 1995, “Calculation of the Temperature Distribution in an Asynchronous Machine”, European Transctions on Electric Power, Vol. 5, No. 3, May/June, 6 p.

12. Responsibility notice

The authors are the only responsible for the printed material included in this paper.